

MAPPING THE EXPOSURE RATE OF GEOGENIC RADIATION IN CAÇAPAVA DO SUL - RIO GRANDE DO SUL, BRAZIL

Felipe Augusto N. Jesus ¹ , Bruna da Luz Farias ² ,
Guilherme Navarro D. Tavares ¹ , Mario Jesus T. Rosales ³ 

ABSTRACT. There are several academic and technical (occupational) types of research about natural radioactive emissions, such as geogenic radon. This field work has gradually broadened in Brazil. In 2019, it was started a project to map the risk of exposure to geogenic radiation was started at the Federal University of Pampa, when the first measurements of radon emission were carried out in the municipality of Caçapava do Sul, Rio Grande do Sul State. In order to continue the project launched in 2019, this current research sought to estimate radiation dose rates and to map the concentration levels of other radioelements (uranium, thorium, potassium) together with the radon measurements, covering the urban area of Caçapava do Sul, and radiation dose estimates. In this case it was possible to verify that the concentration of radon activity was the main responsible for the classification of regions of the study area as exposure scenarios. Based on spatial distribution and concentration data of radioelements, it was identified high emission zones of radiation, from 1 mSv/year to 3 mSv/year in the midwest and north portions of the urban perimeter of Caçapava do Sul, respectively. Exposure to high levels of natural background radiation is an important public health problem.

Keywords: geogenic radiation, Caçapava do Sul Granitic Complex, exposure scenario, ionizing radiation, natural radioactivity

RESUMO. Existem diversas pesquisas acadêmicas e ocupacionais sobre as emissões radioativas naturais de origem geogênica. Em 2019, na Universidade Federal do Pampa, foi iniciado um projeto de mapeamento de risco de exposição à radiação geogênica, quando foram realizadas as primeiras medições de emissão de radônio no município de Caçapava do Sul, Rio Grande do Sul. Com objetivo de dar continuidade ao projeto iniciado em 2019, a presente pesquisa buscou estimar os índices de doses de radiação e mapear os níveis de concentração de outros radioelementos (urânio, tório, potássio) em conjunto com as medidas de radônio, abrangendo a área urbana de Caçapava do Sul. A partir das estimativas de doses de radiação, verificou-se que a concentração de atividade do radônio foi o principal responsável para a classificação de determinadas regiões da área de estudo como cenários de exposição. Com base na distribuição espacial e nos dados de concentrações dos radioelementos, foram identificadas zonas de exposição a níveis de radiação entre 1 mSv/ano e 3 mSv/ano, nas porções centro-oeste e norte do perímetro urbano de Caçapava do Sul, respectivamente. A exposição a altos níveis de radiação natural é um importante problema de saúde pública.

Palavras-chave: radiação geogênica, Complexo Granítico Caçapava do Sul, cenário de exposição, radiação ionizante, radioatividade natural

Corresponding author: felipe.geo95@gmail.com

¹ Universidade de São Paulo (USP) / Serviço Nacional de Aprendizagem Comercial (SENAC), Rua Orense, 41, Sala 808, 09920-650, Centro, Diadema, SP, Brazil – E-mail: felipe.geo95@gmail.com; guilherme.navarro.tavares@usp.br

² Pontifícia Universidade Católica de Minas Gerais (PUC Minas), Belo Horizonte, MG, Brazil – E-mail: brunnapradiefarias@gmail.com

³ Universidade Federal do Pampa (UNIPAMPA), Avenida Pedro Anunciação, 96570-000, Vila Batista, Caçapava do Sul, RS, Brazil – E-mail: mariorosales@unipampa.edu.br

INTRODUCTION

Natural radiation is considered the biggest contributor to the radiation dose received by the world population (UNSCEAR, 2011). Geogenic radioactivity is produced from radioactive elements of minerals present in the Earth's crust: Uranium (^{238}U and ^{235}U), Thorium (^{232}Th), Radium (^{224}Ra), Radon (^{222}Rn), and Potassium (^{40}K), among others. According to Otton (1992), high concentrations of these radioactive elements occur in association with a variety of granitic igneous rocks and related soils. In Brazil, there are several academic and occupational researches at local scale that study subsurface geogenic radioactive activities (Godoy *et al.*, 2011; Campos *et al.*, 2013; Merola and Schenka, 2017; Farias, 2019; Filgueiras *et al.*, 2020).

In 2018, the Geological Survey of Brazil (CPRM) suggested the implementation of the "Brazilian Radon Exposure Risk Program" (Souza Filho and Rocha, 2018) aiming to provide subsidies, at national level, to develop action plans and optimization of cancer care policies with respect to exposure to Radon. According to Filgueiras (2020), there is little research aiming to map natural radioactivity in Brazil. Nonetheless, according to these authors, studies of this nature can support epidemiological and geological correlations, checking if there is a cause-and-effect relationship. Caçapava do Sul is a city in the Center-South portion of Rio Grande do Sul, a Southern Brazilian state. The urban area, where most people live, is located over granitic rocks with an outcrop of approximately 250 km², originally named Caçapava Granitic Batholith, formerly known as Caçapava do Sul Granitic Complex (Nardi and Bitencourt, 1989).

In 2019, the Federal University of Pampa (UNI-PAMPA) started a project entitled "Radon Concentrations in Groundwater and the Exposure Risk for the population of Caçapava do Sul". The project was an initiative to calculate the exposure risk to geogenic radiation, when the first measurements of radon emission were taken in Caçapava do Sul, to verify the relation between the geological context and the gas emission. The results showed that the levels found exceeded the World Health Organization reference values by more than 300% in some places, suggesting that the population would be exposed to a "natural source" of radiation (Farias, 2019).

Following the radiation exposure risk mapping project that started in Caçapava do Sul and supporting a new research about this theme, this study aimed to map the concentration levels of radioactive elements (Uranium, Thorium, Potassium and Radon) in the Caçapava do Sul urban area and a portion of the rural area, through aerogeophysical data combined with radon measurements taken from the project "Radon Concentrations in Groundwater and the Exposure Risk for the population of Caçapava do Sul" project. Additionally, this research provides an estimate of the effective dose rate of geogenic radiation for areas with high concentration levels.

It also evaluated the correlation between the geological characteristics of the region and the concentration levels of the mapped radioactive elements.

STUDY AREA

The study area, delimited by the red rectangle of Figure 1, has approximately 910 km² and covers a large portion of Caçapava do Sul, including the entire urban area and a portion of the rural area. It lies 260 km away from the capital of the state (Porto Alegre), connected by the BR-290 highway. The Caçapava do Sul urban area, highlighted by the dashed line, is the area where the majority of Caçapava's population lives. The total population of the city is estimated at 33,624 inhabitants, according to the demographic data from the Brazilian Institute of Geography and Statistics (IBGE, 2012).

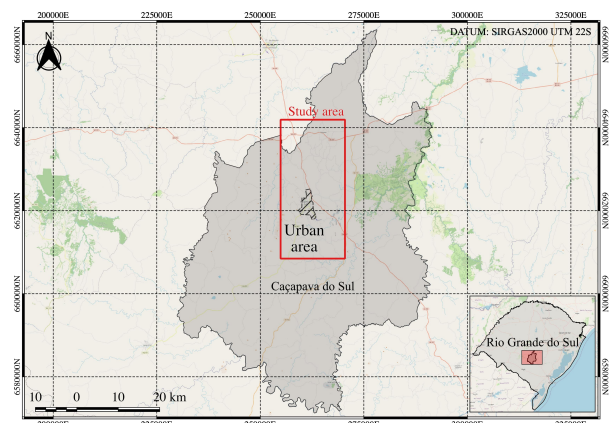


Figure 1. Location map of the study area.

Regarding the description of the geological aspects, Figure 2 shows the geological map of the study area. The most detailed data available for this region are from Folha Caçapava do Sul (1:50,000 scale), mapped in the "Caçapava do Sul Project" by the Institute of Geosciences of the Federal University of Rio Grande do Sul (UFRGS).

The Passo Feio Metamorphic Complex corresponds to the intruded terrain. Dating from the Neoproterozoic (Fragoso-César, 1991), it is composed of the following sequences: magnesian (sm) tremolites and talc-shales of lenticular geometry; chemical metasedimentary (smsq) impure dolomitic marbles, with an olivine content below 10%, serpentinite, clinocllore and talc; clastic metasedimentary (smsc) pelitic schists and phyllites, with centimetric levels of quartzite and localized occurrences of metarenites; intermediate metavolcanic sedimentary (smvi) phyllite and phyllite schist chlorite, with variable quartz content and millimetric intercalations of bands where quartz-carbonate or quartz-plagioclase predominates; and basic metavolcanosedimentary (smvb) amphibole shale and phyllite, homogeneous or finely laminated, massive and banded, massive or lightly foliated metabasites with fine grain and metagabbros.

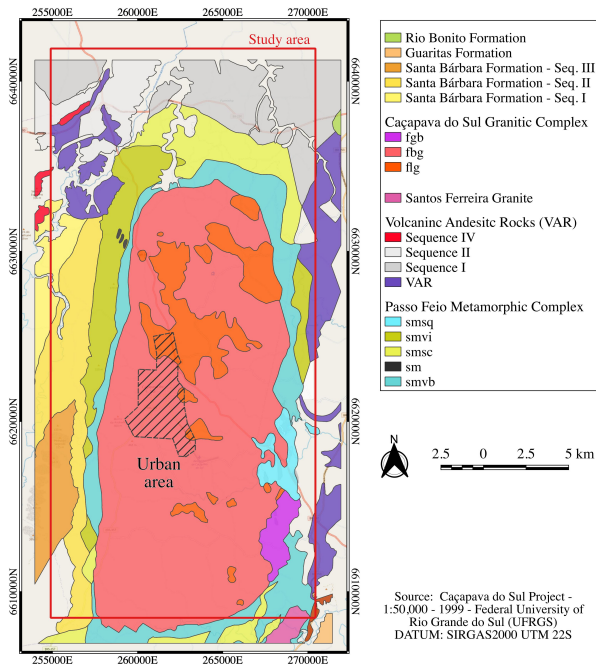


Figure 2. Geologic map of the study area.

The Volcanic Andesitic Rocks (VAR): volcanic package dated from the Cambrian, inserted in the Bom Jardim Group and consisting of thick layers of lava and pyroclastic rocks interspersed in Sequences I, II, III and IV. The VAR are rocks of andesitic composition with rhyolitic porphyritic texture, with the occurrence of tonsils and vesicles, flow structure and subordinate lytic tufts.

The Caçapava do Sul Granitic Complex: Neoproterozoic granitoids, about 552 ma (Nardi and Bitencourt, 1989), weakly foliated in the center of the intrusion, mylonitic on the edges and compound by three recognizable facies - leucogranitoid facies (flg) monzogranites, predominant over syenogranites with an equigranular to medium heterogranular texture, with occurrences of garnet and muscovite; granite biotite facies (fbg) granodiorites to monzogranites of heterogranular to porphyritic texture, mafic content higher than 10%, with a wide predominance of biotite over amphibole; and banded granite facies (fgb) granodiorites to monzogranites, leucogranitoids and rare tonal and dioritic terms, alternated along with the banding on a mesoscopic scale, with mylonitic foliation parallel to the compositional alternation.

The Santa Bárbara Formation: conglomerates with cross-stratification, variable-sized immature sandstones, feldspathic greywacke, siltstones and claystones interspersed among Sequences I, II and III, dating from the Cambrian, member of the Camaquã Group.

The Guaritas Formation: alluvial fan facies association, polymictic conglomerates with angular to rounded clasts, with lenticular geometry and fluted cross stratification, poorly selected sandstone, of very dark red color and presence of paleocurrent structures, dating from the end of the Cambrian, member of Camaquã Group.

The Rio Bonito Formation: conglomerates that scale to fine sandstones of lenticular geometry and medium-sized planar crossed stratification, with a wavy, hummocky and linsen structures and bioturbation, siltstones with rhythmic levels and very fine sandstone lenses, layers of coal and carbonaceous shales, dated from the Permian, member of the Guatá Group.

METHODOLOGY

Transport of Natural Radiation and Exposure Indexes

In the environment, radioactive substances travel through several compartments, known as transfer routes, until they reach the human receptor (Mazzilli *et al.*, 2011). These exposure pathways are often used to calculate radiation doses due to certain sources and routes.

Through the quantification of concentrations of radioactive elements in a certain area of interest and definition of exposure parameters, it is possible to determine exposure rates, also called radiation doses. Thus, the final value must be compared to an acceptable risk level. Therefore, it is possible to calculate these indexes through potassium concentrations (in %), thorium equivalent, and uranium equivalent (both in ppm), obtained through aerial surveys, in addition to the concentration of Radon activity, obtained through radiochemical tests (Godoy *et al.*, 2011).

Eq. (1) describes the Effective Dose of radon due to water ingestion (EDIG), according to the UNSCEAR model (Mittal *et al.*, 2016), where the average concentration of Radon activity (C) is weighted against a water consumption factor (C_w) and an Effective Dose Coefficient (EDC) for ingestion.

$$EDIG = C \times C_w \times EDC \quad (1)$$

Where C_w is the number of liters ingested within a 1-year interval (≈ 60 l) and EDC is equal to 3.5 nSv Bq^{-1} .

Eq. (2) describes the Effective Dose of radon due to inhalation (EDIH) of radon released from water into air, according to the UNSCEAR model (Mittal *et al.*, 2016), where the average concentration of Radon activity (C) is weighted against a ratio of radon in air to radon in tap water (R_w), an equilibrium factor (F), an occupancy factor (O) and a Dose Conversion Factor (DCF).

$$EDIH = C \times R_w \times F \times O \times DCF \quad (2)$$

Where R_w is equal to 10^{-4} , F is the equilibrium factor between radon and its decay products (0.4), O the number of hours contained within a 1-year interval that people would be exposed to radon activity (7000 h) and DCF is equal to 9 nSv h^{-1} .

Eq. (3), taken from the work of Godoy *et al.* (2011), describes the Annual Dose Radiation Index (ADRI), quantified from the work of Grasty *et al.* (1984), assuming a constant factor of 320 related to cosmic ra-

diation (mainly from solar activity) and considering the concentrations of the radioelements Uranium, Thorium and Potassium, according to their respective contributions.

$$ADRI = 320 + 52,56 \times [(K \times a) + (U \times b) + (Th \times c)] \quad (3)$$

Where $a = 1,505$, $b = 0,625$ and $c = 0,310$. Table 1 presents limits established by the International Commission on Radiological Protection (ICRP), which considers the exposure scenario of the common public (population). Also, according to the ICRP, when considering a public exposure scenario, the dose limits apply to the sum of the exposure sources, that is, the sum of the indexes calculated through Eq. (1), Eq. (2) and Eq. (3).

Table 1. Exposure scenario classification and dose limits.

Classification	Dose limit
Considered exposure scenario	1 mSv/year
Residential exposure scenario	3-10 mSv/year
Plausible intervention	>10 mSv/year
Eye exposure	15 mSv/year
Skin exposure	50 mSv/year
Justifiable intervention	100 mSv/year
Reallocation	>100 mSv/year

Source: adapted from [Valentin et al. \(2007\)](#).

Correlation between Geology and Natural Radiance

As mentioned before, variation in the concentration of radioactive elements can be influenced by the geological structure of the area. This influence demonstrates the concept of dependence, which is when the variation of the first variable (natural radiation) depends on the second variable (outcropping lithology).

Several studies demonstrate the dependent relationship between natural radiation and the lithology of a given terrain ([Godoy et al., 2011](#); [Szabó et al., 2014](#); [Ciotoli et al., 2017](#); [Ribeiro et al., 2017](#); [Filgueiras et al., 2020](#)). Among the various approaches, the box diagram comparison proved to be a versatile tool to analyze the concentration of radiation activity in terrain from different geological formations.

In the work of [Ribeiro et al. \(2017\)](#), the exploratory analysis of the box diagrams demonstrated variation in the concentration of Radium (^{226}Ra and ^{228}Ra) and Potassium (^{40}K) in different geological formations in the Fernando de Noronha Archipelago. In the work of [Szabó et al. \(2014\)](#), the analysis of the box diagrams revealed that a higher concentration of ^{222}Rn activity in the soil occurs in mountains and hills compared to the plains. Through the analysis, the authors also

demonstrated that, in addition to the geological formation, the ^{222}Rn concentrations were also related to the weathering of rocks and sediment generation in the study area.

Spatial Continuity and Phenomenon Modeling

The natural properties of the Earth's surface are spatially continuous, so its descriptions, through simple mathematical functions, become restricted ([Camargo, 1998](#)). To represent the natural phenomena associated with the surface properties, such as geogenic radiation, mathematical models called Numerical Terrain Models (NTM) are used. The generation of NTMs goes through 3 stages ([Camargo, 1998](#)): sampling, modeling and application.

Sampling comprises the acquisition of a set of samples representative of the phenomena of interest. Modeling involves the generation of surfaces of continuous representation of the phenomenon from the samples, usually through regular grids or blocks generated by the interpolation method. Application corresponds to the analysis procedure performed on the NTM.

Regarding the modeling of the phenomenon, specifically on interpolation, it is a process used to estimate the value of an attribute in non-sampled locations using sampling points obtained in regions close to those that will have their estimated values ([Santos et al., 2016](#)). In the case of spatially continuous phenomena, inferential models such as Kriging ([Camargo, 1998](#)) and Nearest Neighbor Analysis are used.

Database

The work development used four different categories of data (Fig. 3): Rn concentration activity given in Bq/l; radioelement concentration given in % (K) and ppm (eTh and eU); geological information that includes lithological characteristics of the region of interest; and Caçapava do Sul population housing characteristics.

Regarding the Rn activity concentration data, the database obtained from the project "Radon Concentrations in Groundwater and the Exposure Risk for the population of Caçapava do Sul" (2019) was used, available in table format with the position information and concentration value of each sample collected (Fig. 3).

Concentration measurements were obtained from 100 ml water samples injected into the AlphaGUARD degassing unit, measuring the concentration every minute until stability (about 3 minutes). After stability, the water circulated within the AlphaGUARD system for 10 minutes and effective measurements were carried out for the next 10 minutes (no water circulation). After this measurement process, the dilution effect was removed from effective measurements through Eq (4).

$$C = \frac{C_L \times \left(\frac{V_A - V_s}{V_s} + k \right) - C_0}{1000} \quad (4)$$

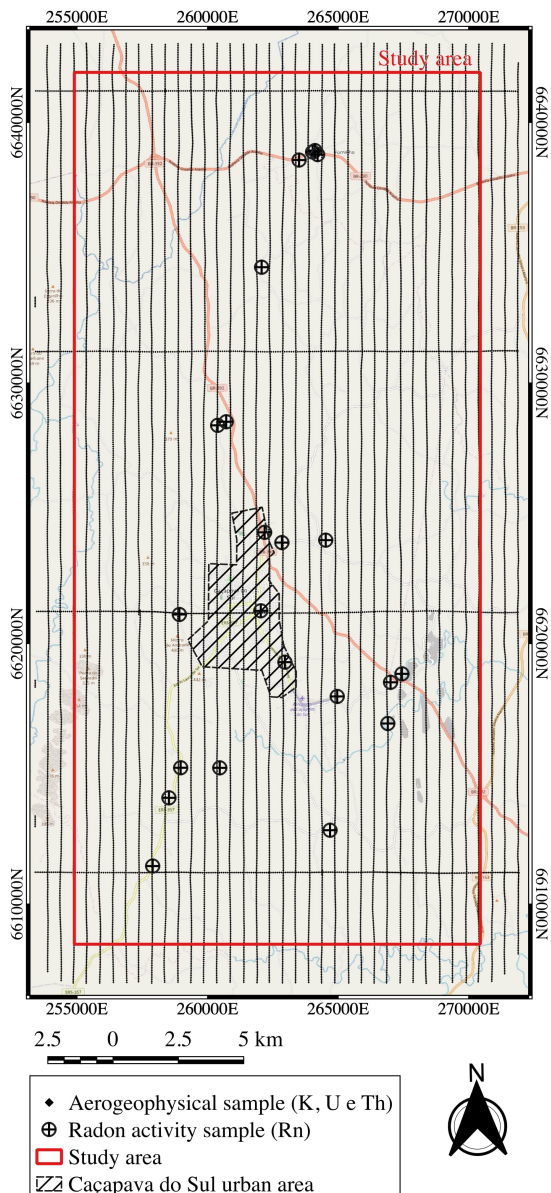


Figure 3. Location map of the samples used in the development of this research.

Where C is the Rn concentration activity, C_L is the Rn concentration activity after degassing, V_A is the Alpha-GUARD unit volume (1122 ml), V_s is the water sample volume, k is a temperature contribution factor equal to 0.26 and C_0 is the Rn concentration activity before the measurement equal to 0.

Regarding the concentration data of the radioelements eU, eTh and K, the database available by CPRM geoserver was used - "Projeto Aerogeofísico Escudo do Rio Grande do Sul" (2009), available in two files in vector format, corresponding to the flight lines and the control lines of the aerial survey, containing the position and concentration value of each sampled point. The flight lines correspond to parallel lines spaced 500 m apart with N-S direction. The control lines correspond to parallel lines spaced 10 km apart, with an orthogonal direc-

tion to the flight lines, therefore, E-W. Both acquisitions were made at a height of 100 m. The data were cut over the limit of the area, as shown in Fig. 3, to intentionally avoid contour problems during data processing.

The vector base of census sectors made available by the Brazilian Institute of Geography and Statistics (IBGE) was used to verify characteristics of the housing units of Caçapava do Sul. The sectors classified as "urban" were selected to delimit the urban perimeter of the municipality.

Statistical Analysis

For statistical analysis of the data, we chose to use the graphs of box diagrams and the basic parameters of the classic descriptive statistics, below the list of steps and the tools used in the generation of the products.

The libraries NumPy, GeoPandas, Seaborn and Matplotlib in Python and software QGIS were used as tools.

On the first approach, the routine of Basic Statistics for Attributes, in QGIS, was used to calculate the main statistical parameters of each database, which correspond to the total number of samples, mean, median, quartiles, maximum, minimum and standard deviation.

On the second approach, we applied the Spatial Join routine, in QGIS, to unite the attributes of the geological description layer of the study area with the layers corresponding to the samples of radioelements, where each sample was linked to the lithotype corresponding to its collection position.

After linking samples and lithotypes, the linked data were imported into the python environment, where the boxplots were generated. In the boxplot generation, the lithotype linked to each sample was assigned to the X-axis while the concentration measurements of each radio element were assigned to the Y-axis of each graph.

Geostatistical Analysis

For geostatistical analysis of the data, histograms, semi-variograms and processing routines for data interpolation were used. The list of steps and tools used in the generation of the products is below.

The libraries NumPy, SciPy, GeoPandas, Matplotlib and Scikit-gstat in Python and software QGIS were used as tools.

The histograms were developed with the vector bases imported into the python environment and made possible the evaluation of the concentration distribution concerning the parameter of skewness. In this step, the distributions of the bases were tested before and after the logarithmic transformation, where the distribution of greater symmetry (or less asymmetry) started to be used in the next processing steps.

After the step of assessing the distribution of concentrations of the data, the Nearest Neighbor Analysis in the QGIS routine was used to evaluate the spatial distribution pattern of the sample sets to estimate input parameters for spatial modeling. In the average distances observed, the samples of each set were used as inputs

to increase the lag distance of the semi-variograms, while half of the maximum distance observed among samples of the same set was used as an adjustment limit.

The experimental semi-variograms were built after the symmetry analysis. In this step, we sought to adjust the parameters of threshold, reach, and nugget effect of all experimental semi-variograms of the sample sets.

The semi-variograms adjustment was made considering isotropic models and a regression routine based on the Matheron method (Matheron, 1962). Based on the adjustment of semi-variogram parameters, an analysis of spatial dependence of each sampled phenomenon was made based on the work of Cambardella et al. (1994), i.e., the Spatial Dependence Index (SDI) values below 25% indicate strong spatial dependence, values between 25% and 75% indicate moderate dependence, while values above 75% indicate weak spatial dependence.

Based on the adjusted experimental semi-variogram, the interpolation of the sample sets was performed using the Ordinary Kriging method. In this step, a 100 x 100 m grid was standardized as the size of the cells in the output file and the edges of the study area were assumed as the spatial limit of the interpolation. After interpolation, the files were exported in a matrix format (.TIFF) for handling in QGIS.

After importing the interpolated matrix data into QGIS, a cross-validation routine was applied to check the accuracy of the interpolations, where scatterplot graphs were generated as linear adjustments comparing the modeled values and observed values, samples estimated values and residual of the difference between observed and estimated values.

RESULTS

Statistical Analysis

The results obtained in this research are presented together with comments and critical analyses of the products generated during each stage.

Table 2 summarizes the results obtained through classical descriptive statistics for data on Rn activity concentration, eU concentration, eTh concentration, and K concentration.

Table 2. Descriptive statistics of radioelement samples, where μ is mean, M is median and σ is the standard deviation.

Element	Max	Min	μ	σ	M
Rn (Bq/l)	322.56	10.50	83.76	92.16	34.04
eU (ppm)	3.90	-1.70	0.89	0.49	0.84
eTh (ppm)	32.19	0.86	6.88	2.87	6.50
K (%)	6.21	0.00	2.33	1.16	2.14

The similarity between the mean (μ) and the median (M), as seen in the case of eU, eTh and K samples, suggests a normal distribution for these variables. This pattern is more evident when evaluating the histograms of these sets (Figs. 4b, 4c and 4d), where the asymmetry values are close to 0 and the distribution curve visibly behaves like the Gaussian (normal) distribution.

In the set of Rn samples there is a great variability as this pattern is evidenced by a standard deviation greater than the mean and the difference between the mean and the median. In addition, the high variability in the set of Rn samples is more evident when looking at the histogram of this set (Fig. 4a), where an asymmetry value away from 0 and a visibly different curve is noted from the Gaussian curve. In the case of sets with high variability of Rn activity concentration, the use of logarithmic transformation can be an approach to standardize the values (Ciotoli et al., 2017), reducing the variability and increasing the symmetry, which benefits the variogram adjustment.

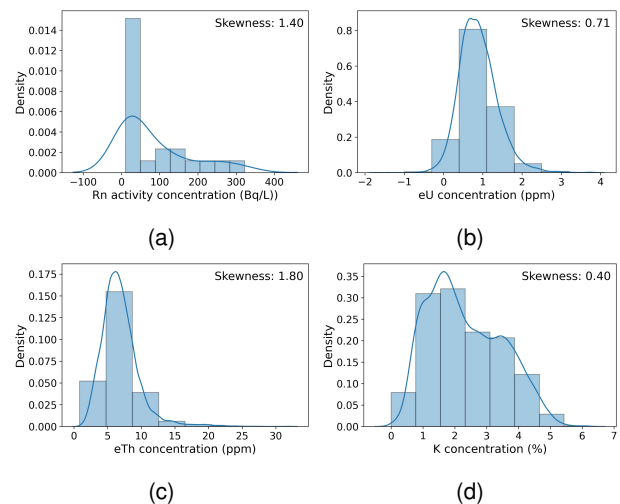


Figure 4. Sample set histograms of (a) Rn activity concentration, (b) eU concentration, (c) eTh concentration and (d) K concentration.

As shown in Figure 5, the boxplot of the set of Rn activity samples as a function of the different lithologies, linked to the collection points, highlights that lithologies have different concentration distributions.

It is possible to see that the two facies of the Caçapava do Sul Granitic Complex have higher concentrations than the VAR and smsq of the Passo Feio Metamorphic Complex, with the flg facies concentrating the highest measured values. Also, through the boxplot, it can be seen that in the same lithology, the two facies, flbg and flg, have different concentration ranges. These differences in the distribution of concentration reflect the variation in composition between one lithology and the other, and could even reflect small variations in the same lithology.

Figure 6 shows the boxplot of the set of samples of concentration of eU as a function of the lithotypes

linked to the collection points. In this case, it is observed that the set of samples includes 18 different lithologies, which vary in terms of lithotypes, facies, and stratigraphic sequence.

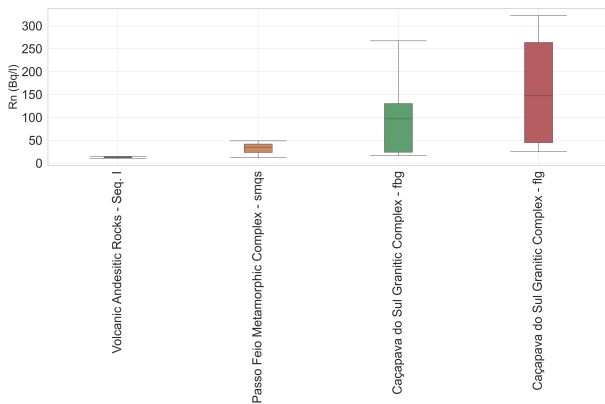


Figure 5. Rn concentration boxplot as function of lithotypes from the study area.

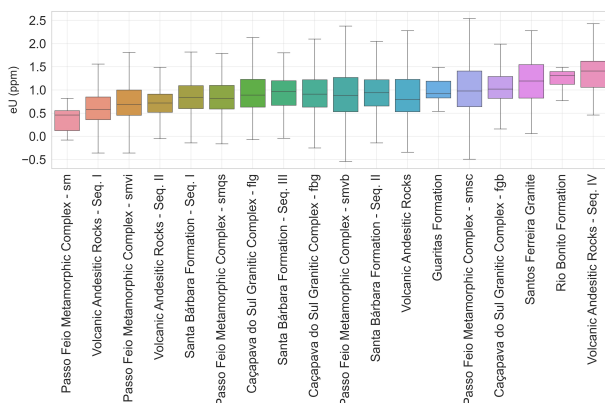


Figure 6. U concentration boxplot as function of lithotypes from the study area.

Despite the number of lithologies, in most groups, 13 of 18, the medians remained in a value range close to 1 ppm. In addition, the median eU concentrations, presented in ascending order, indicate that there is no pattern directly associated with the lithological type, since different VAR sequences are found at extreme points in the diagram (VAR Sequence I and VAR Sequence IV).

Figure 7 presents the boxplot of the set of eTh concentration samples as a function of the lithotypes linked to the collection points. These results are similar to those reported above, and it includes the same 18 lithotypes mentioned before, however, a greater variation range is noted among the 18 clusters. Medians range from 4 ppm to approximately 10 ppm. Additionally, the results are similar to eU concentrations. There is no apparent pattern of association between lithotype and eTh concentration, since different sequences of VAR and Passo Feio Metamorphic Complex are found at extreme points in the diagram.

Figure 8 presents the boxplot of K% concentration sample set as a function of those 18 lithological groups already mentioned. For instance, as observed from the activity of Rn, there is a pattern between the distribution of concentration and the lithological clusters.

It is remarkable in Figure 8 the Granite Complex of Caçapava do Sul, a dominance of the highest medians of all the subsets (three out of four), two above 3% concentration. At the other edge of the boxplot, the intermediate composition lithologies (VAR - Sequence I, Metamorphic Complex - smsc) to the basic one (Metamorphic Complex - sm and smvb) have the lowest medians of the clusters. This behavior reflects the compositional characteristics of the lithotypes, since granites correspond to intrusive acid rocks with a potassium minerals predominance, while rocks of intermediate to basic characteristics are enriched in mafic minerals and have a lower potassium concentration.

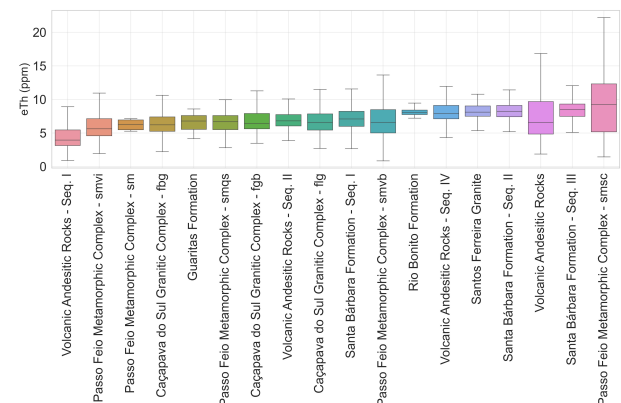


Figure 7. Th concentration boxplot as function of lithotypes from the study area.

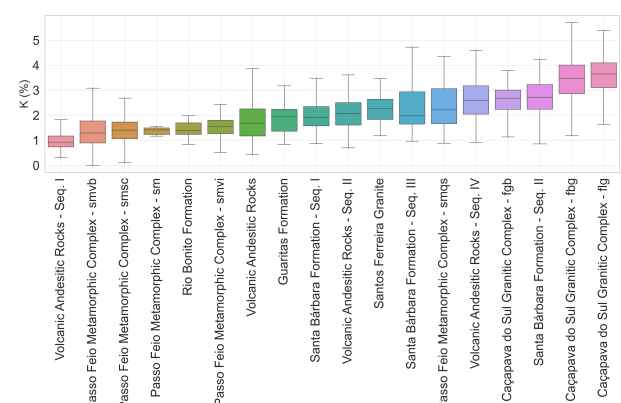


Figure 8. K concentration boxplot as function of lithotypes from the study area.

Spatial Analysis

Table 3 summarizes the results obtained from the distance analysis of the Rn activity sample sets and the cut set of aerial survey samples with the eU, eTh and K concentrations.

Table 3. Distance analysis of sample sets, where *n* is the counted number of samples.

Set	<i>n</i>	Max (m)	Expected mean (m)	Observed mean (m)
Rn activity	22	28,160	1,725	1,494
K, eU eTh	17,320	39,730	88	65

The maximum distance between collection points in both sets is close to 30,000 m. Based on this distance, Table 4 shows the parameters of the semi-variograms adjusted for the maximum Lag distance of 15,000 m (Fig. 9), adopting the isotropic spherical model.

Table 4. Adjusted semi-variograms parameters.

Set	<i>r</i> ²	Sill	Nug. effect	IDE
Rn (Bq/l)	60%	1.92	3.6×10^{-10}	$2 \times 10^{-8}\%$
eU (ppm)	84%	0.23	0.13	59%
eTh (ppm)	91%	0.13	0.02	18%
K (%)	98%	1.34	0.11	8%

The semi-variogram adjusted for the concentration of Rn activity (Fig. 9a) indicates that after 15,000 m the samples have no correlation, which corresponds to the limit of the maximum Lag distance used in the adjustment. The threshold, after the log scale transformation, indicates that 83.37 (Bq/l)^2 is the stabilization value for variance as a function of the Lag increment. SDI less than 25% indicates a strong spatial dependence on the phenomenon.

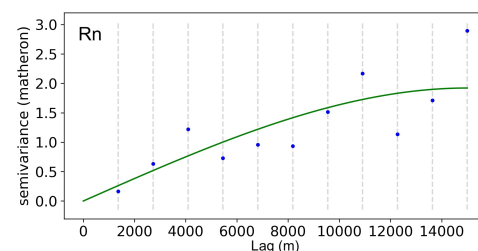
The semi-variogram adjusted for the eU concentration (Fig. 9b) indicates that after 3,700 m the samples are not correlated, approximately 1/4 of the range used for the adjustment. The threshold indicates that 0.228 ppm^2 is the stabilization value for variance as a function of the Lag increment. SDI less than 25% indicates that the phenomenon has a strong spatial dependence.

The semi-variogram adjusted for the eTh concentration (Fig. 9c) indicates that after 3,800 m the samples are no longer correlated, a value close to that found for modeling the eU concentration. The threshold indicates that 0.125 ppm^2 is the stabilization value for variance as a function of the Lag increment. SDI less than 75% indicates that the phenomenon has moderate spatial dependence.

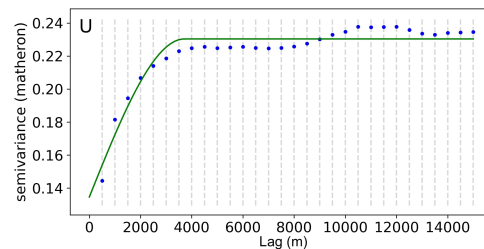
The semi-variogram adjusted for the concentration of K (Fig. 9d) indicates that after 8,800 m the samples are no longer correlated, about 3/5 of the maximum range used in the adjustment. The threshold indicates that 1.344 ppm^2 is the stabilization value for variance as a

function of the Lag increment. SDI less than 25% indicates that the phenomenon has strong spatial dependence, in this case, dealing with the phenomenon with the strongest dependence among all.

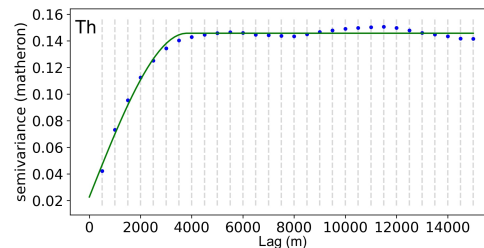
The range of each semi-variogram differs, which suggests that the modeled phenomena have distinct spatial correlations. The SDI obtained for each semi-variogram reinforces the first point observed and suggests that the spatial dependence of each phenomenon is different. All the determination coefficients (*r*²) stayed above 60% in all models, which suggests a good fit of the isotropic spherical model to represent the spatial variation of the phenomena.



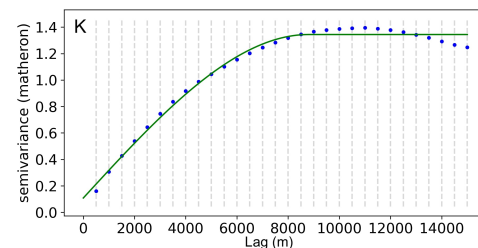
(a)



(b)



(c)



(d)

Figure 9. Adjusted semivariograms to the set of samples of (a) Rn activity concentration, (b) eU concentration, (c) eTh concentration, and (d) K concentration.

Figure 10 shows the isovalue maps of the radioelements analyzed, while Figure 11 shows the linear adjustment of the isovalues to the observed data and their respective residuals. The maps allow the visualization of the spatial distribution of radioelements in a continuous way in the study area and are presented with false color scales. Warm colors indicate higher concentrations while cold colors indicate lower concentrations.

Figure 11 presents the cross-validation graphs, where the adjustments and residuals (differences) are observed, in terms of the coefficient of determination (r^2) of the concentration values estimated by the models as a function of analytic values (samples). In all cases, the linear adjustment of the estimated measures in relation to the observed measures presents slopes close to 1 and r^2 above 0.9, which indicates that the estimated values represent more than 90 % of the values observed by the samples.

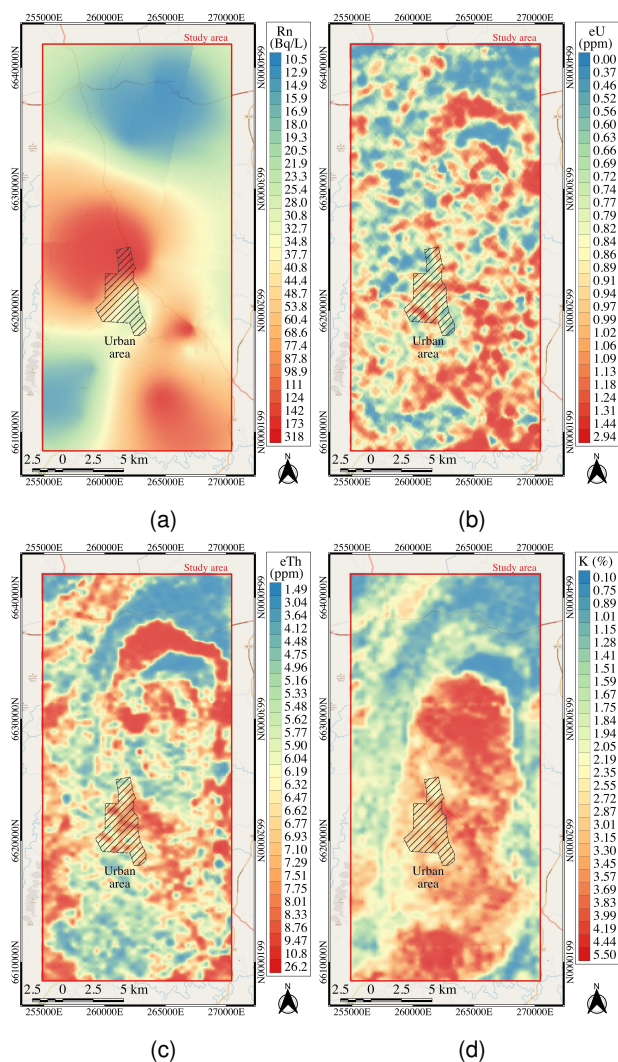


Figure 10. Isovvalue maps of (a) Rn activity concentration, (b) eU concentration, eTh concentration, and (d) K concentration.

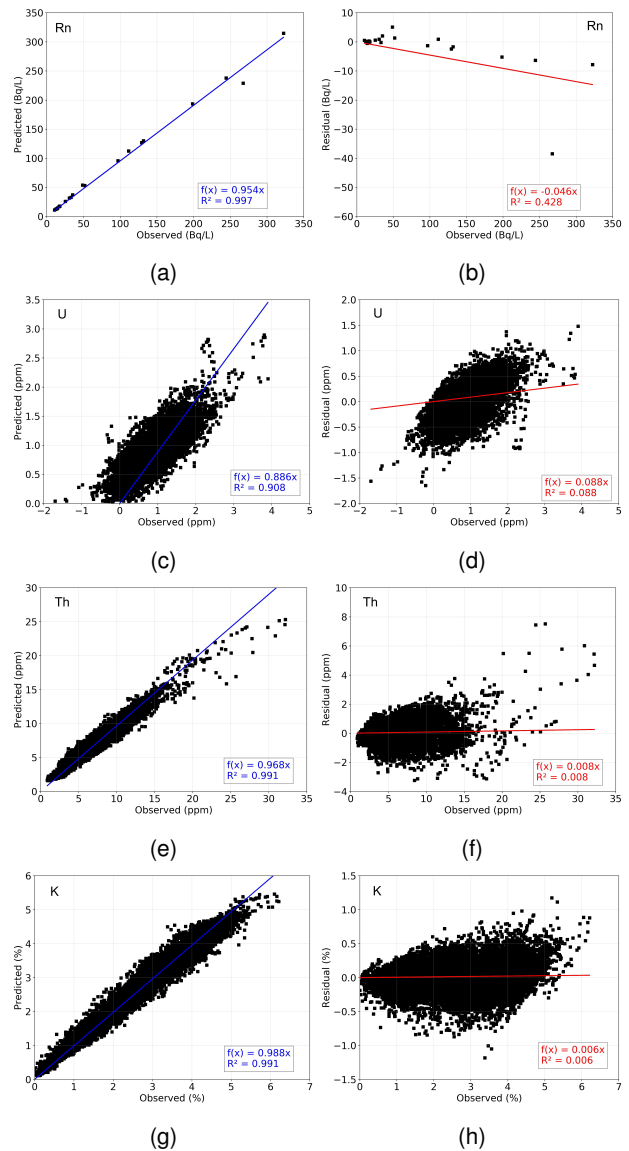


Figure 11. Cross-validation graphs showing the adjustment of model predicted values in relation to observed (a) Rn activity concentration, (c) eU concentration, (e) eTh concentration, (g) K concentration and related residues in (b), (d), (f), and (h).

Regarding the residual analysis, it is observed that all graphs show linear adjustments with slopes close to 0, however, when checking the r^2 it is observed that the adjustment of the Rn and eU measurements shows values of 0.428 and 0.088, respectively, while for eTh and K the values remain below 0.01. This difference may be associated with the low number of Rn samples used in the adjustment of the model and the portion of randomness in the spatial distribution of the phenomenon, as the eU case.

Estimated Radiation Doses

Currently, the acceptable risk of additional cases of cancer ranges from 1:100,000 to 1:1,000,000, according to local legislation (CETESB, 2017; USEPA, 2021), either

for radioactive sources as well as soil and groundwater contamination. According to ICRP (2005), the current 1 mSv annual dose limit to the members of the public (ICRP, 2007) exceeds the acceptable risk by five times. Therefore, it is not a conservative limit, but it was defined under pressure from the nuclear industry (ICRP, 2005).

According to the results presented in Figure 12, the members of the public (residents of the urban area of Caçapava do Sul) are exposed to a dose of 3 mSv/year. This dose lies between the lower limit (1 mSv/year) and the maximum limit (20 mSv/year) for natural background radiation (ICRP, 2007), characterizing potential risk since there is an increase in cancer cases for these receptors (members of the public, workers and patients).

Considering the limits established by Valentin *et al.* (2007) (Table 1), it is an area already considered as a potential exposure scenario. However, prior to any interventions, the items below should be evaluated and considered:

- The existence of real risk based on direct measurements obtained in the field;
- The existence of real risk based on epidemiological data, since it is an existing exposure situation;
- The principle of justification (ICRP, 2007).

According to the results presented in Figure 12b from the north peripheric region of Caçapava do Sul, there are zones with values above 1 mSv/year. These zones, corresponding to the Valentin *et al.* (2007) limits (Table 1), report doses under the domestic scenario limit, not reaching levels that justify intervention. However, these values exceed the reference level established by ICRP (2007). In this way, they are zones whose real risk should also be assessed, and whose epidemiological results cannot be used as zones that are not impacted during the assessment of real risk.

The other areas evaluated do not present doses above 1 mSv/year. Thus, the potential risk for these areas is not characterized. Also, the epidemiological and direct radon measurement results can be used as a background for non-impacted areas.

In Figure 12c, it is verified that the ADRI in the study area is mainly influenced by the concentrations of K and eTh. It appears that the urban perimeter is composed by a region with doses ranging from 0.6 to 0.9 mSv/year and, when compared to the limits established by Valentin *et al.* (2007) and ICRP (2007), there is no potential risk. However, assuming that the two indexes correspond to portions of a total radiation to which the same area is exposed, both can be combined in a direct sum.

Figure 12d shows the result of the combination of EDIG, EDIH and ADRI indexes, reclassified according to the scenarios indicated by Table 1 (Valentin *et al.*, 2007; ICRP, 2007), where it is noted that the concentration of Rn activity represents the main contribution for

a final risk value, and should be prioritized in the adoption of appropriate mitigation measures.

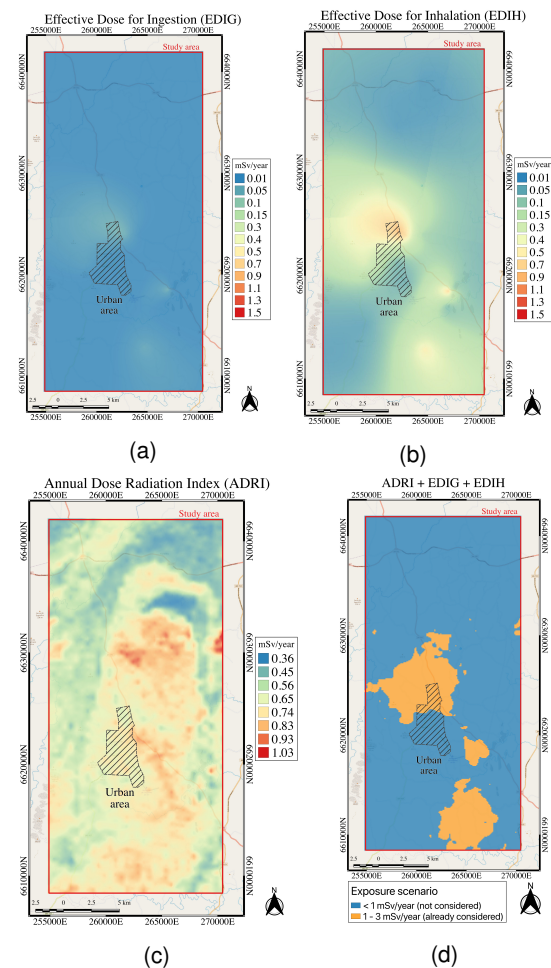


Figure 12. Isovalue maps from estimated a) EDIG, b) EDIH, c) ADRI, and d) sum of the indexes reclassified according to exposure scenarios from Table 1.

CONCLUSIONS

Based on the results obtained in this research it was possible to conclude that: Among the 4 lithological types contemplated by the Rn activity sample set, the Caçapava do Sul Granitic Complex flg facies showed the highest Rn activity concentrations, with maximum values exceeding 300 Bq/l, which is above the domestic effective dose recommendation, according to ICRP (2018). In relation to the eU, among the 18 subsets of samples linked to the lithotypes, in general, the medians remained in a value range close to 1 ppm, whereas in relation to the eTh, the medians would vary between 4 and 10 ppm. Regarding K, it was possible to verify the influence of the Caçapava do Sul Granitic Complex on the concentration levels. It was observed that the 4 granite facets had a median close to or above 3%, while lithotypes of more basic composition, such as VAR Sequence I, presented concentration medians close to 1%. All adjusted semi-variograms had r^2 above 60%,

demonstrating good fit of the spherical isotropic model in spatial variation representation of the modeled phenomena. The range of the adjusted semi-variograms varied among themselves, suggesting that the modeled phenomena have different patterns of spatial correlations, which is expected in function of different natural geochemical patterns of the elements and can be verified through the IDEs of each semi-variogram.

Among the modeled phenomena, the concentrations of eTh, K and Rn activity showed a strong spatial dependence, while the concentration of eU showed a moderate dependence. Different spatial distribution patterns were verified for the interpolations of each data set.

The Rn activity map showed a smooth and homogeneous pattern, while the eU map showed a heterogeneous distribution with several intercalations between high and low concentrations. Th and K concentration maps showed a greater correlation with the lithological limits of the study area. These differences were already expected because there were few samples of Rn and it was necessary to expand the search range for interpolation, whereas the aerogeophysics sets have a larger sample number and, therefore, a higher spatial resolution.

The set of samples used in this work suggests the presence of radiation exposure area levels between 1-3 mSv/year within the urban perimeter of Caçapava do Sul. Based on the results presented and the reference levels considered (ICRP, 2007; Valentin *et al.*, 2007), the potential risk for the considered recipients was identified.

Therefore, the existence of real risk arising from natural background radiation and possible additional cases of cancer in residents of the identified area should be assessed. This investigation should be conducted based on the epidemiological information from affected and unaffected areas, and dose-response assessment, in order to examine the relationship between exposure and effects, in addition to direct measures taken in the field regarding the annual dose emission.

If the real risk for public exposure is confirmed, the total exposure of the workers of this region must be assessed. If the man-made radiation exposure is potential relevant, those workers may require exposure reduction due to their professional activities in order to achieve an acceptable risk, following the principle of optimization of protection (ICRP, 2007).

With the possibility of the existence of a real risk to any receiver, mitigation strategies must be implemented, considering the principle of justification (ICRP, 2007), which states that any decision that alters the radiation exposure situation should bring more benefits than harm.

REFERENCES

Camargo, E.C.G. Geoestatística: fundamentos e aplicações. *Geoprocessamento para projetos ambien-*

- tais. São José dos Campos: INPE* **1998**, p. 36.
- Cambardella, C.A.; Moorman, T.B.; Novak, J.; Parkin, T.; Karlen, D.; Turco, R.; Konopka, A. Field-scale variability of soil properties in central Iowa soils. *Soil Science Society of America Journal* **1994**, *58*, 1501–1511.
- Campos, T.; Petta, R.; Pastura, V.; Sichel, S.; Motoki, A.; Malanca, A. O gás radônio doméstico e a radioatividade natural em terrenos metamórficos: o caso do município de Lucrecia (Rio Grande do Norte, Brasil) **2013**. *26*, 85–93.
- CETESB. 038/2017/C, DE 07 DE FEVEREIRO DE 2017 **2017**.
- Ciotoli, G.; Voltaggio, M.; Tuccimei, P.; Soligo, M.; Pasculli, A.; Beaubien, S.; Bigi, S. Geographically weighted regression and geostatistical techniques to construct the geogenic radon potential map of the Lazio region: A methodological proposal for the European Atlas of Natural Radiation. *Journal of Environmental Radioactivity* **2017**, *166*, 355–375.
- Farias, B.L. *Concentração de Radônio nas Águas Subterrâneas e o Risco de Exposição para a população de Caçapava do Sul - RS*; UNIPAMPA, 2019; p. 61.
- Filgueiras, R.A.; Silva, A.X.; Ribeiro, F.C.A.; Lauria, D.C.; Viglio, E.P. Baseline, mapping and dose estimation of natural radioactivity in soils of the Brazilian state of Alagoas. *Radiation Physics and Chemistry* **2020**, *167*, 108.
- Fragoso-César, A. Tectônica de placas no Ciclo Brasileiro: As orogenias dos Cinturões Dom Feliciano e Ribeira no Rio Grande do Sul: Unpubl **1991**. p. 387.
- Godoy, L.C.; Bittencourt, A.V.; Santos, L.J.; Ferreira, F.J. Distribuição de K, eU e eTh e avaliação da dose anual de radiação na região do Granito Serra do Carambeí-PR. *Revista Brasileira de Geofísica* **2011**, *29*, 359–375.
- Grasty, R.; Carson, J.; Charbonneau, B.; Holman, P. Natural background radiation in Canada **1984**. p. 49.
- IBGE. Censo Demográfico do Brasil de 2010 **2012**.
- ICRP. 2005 ICRP Recommendation, 2005.
- ICRP. ICRP Publication 103 - The 2007 Recommendations of the International Commission on Radiological Protection. *Ann ICRP* **2007**, *37*, 2.
- ICRP. Summary of ICRP Recommendations on Radon, 2018.
- Matheron, G. *Traité de géostatistique appliquée* **1962**. p. 171.
- Mazzilli, B.P.; Máduar, M.; Campos, M. Radioatividade no meio ambiente e avaliação de impacto radiológico ambiental. *São Paulo: IPEN* **2011**, p. 92.
- Merola, Y.L.; Schenka, A.A. Radiação natural e células tronco de tumores mamários em população residente no município de Poços de Caldas-MG **2017**. p. 120.
- Mittal, S.; Rani, A.; Mehra, R. Radon levels in drinking water and soil samples of Jodhpur and Nagaur districts of Rajasthan, India. *Applied Radiation and Isotopes* **2016**, *113*, 53–59.
- Nardi, L.V.S.; Bitencourt, M. Geologia, petrologia e

- geoquímica do Complexo Granítico de Caçapava do Sul, RS. *Revista Brasileira de Geociências* **1989**, 19, 153–169.
- Ribeiro, F.C.; Lauria, D.d.C.; do Rio, M.A.; da Cunha, F.G.; de Oliveira Sousa, W.; Lima, E.d.A.M.; Franzen, M. Mapping soil radioactivity in the Fernando de Noronha Archipelago, Brazil. *Journal of Radioanalytical and Nuclear Chemistry* **2017**, 311, 577–587.
- Santos, H.S.; Cunha, G.N.; Castro, J.R. Avaliação Qualitativa das Técnicas de Interpolação de Mínima Curvatura, Krigagem e Bidirecional na Formação de Imagens. *Revista de Engenharias da Faculdade Salesiana* **2016**, pp. 2–16.
- Souza Filho, O.A.; Rocha, Z. Programa de Risco de Radônio para o Brasil. *Anais do VIII Simpósio Brasileiro de Geofísica* **2018**.
- Szabó, K.Z.; Jordan, G.; Horváth, Á.; Szabó, C. Mapping the geogenic radon potential: methodology and spatial analysis for central Hungary. *Journal of Environmental Radioactivity* **2014**, 129, 107–120.
- UNSCEAR. UNSCEAR 2008 Report: Sources and effects of ionizing radiation. *New York: The United Nations Scientific Committee on the Effects of Atomic Radiation* **2011**.
- USEPA., 2021.
- Valentin, J.; BOICE JR, J.; Clarke, R.; Cousins, C.; Gonzalez, A.; Lee, J.; Lindell, B.; Meinhold, C.; METTLER JR, F.; Pan, Z. Published on behalf of the International Commission on Radiological Protection **2007**.

F.A.N.J.: contributed with the construction of data processing programs, results analysis and description, maps and figures creation, and was responsible for structuring and submitting the article. **B.L.F.:** contributed with the acquisition of radon emission measurements, writing the geological aspect text and building the problem contextualization. **G.N.D.T.:** contributed with discussions and criticisms about the statistical and spatial data analysis. Also reviewed the geological aspect description of the study area and brought a critical view on the risk of exposure to natural radiation. **M.J.T.R.:** due to his wide experience, contributed with a general and critical view of the work and with the initial proposal of investigating natural radiation levels in Caçapava do Sul.

